Surface melt at SIGMA-B site in Qaanaaq Ice Cap, northwestern Greenland triggered by radiant fluxes in the 2015, 2019, 2020 summers

Motoshi Nishimura[1], Teruo Aoki[1], Masashi Niwano[2], Sumito Matoba[3], Tomonori Tanikawa[2], Satoru Yamaguchi[4], and Tetsuhide Yamazaki[5]

[1]*Arctic Environmental Research Center, National Institute of Polar Research*

[2] *Meteorological Research Institute, Japan Meteorological Agency*

[3] *Institute of Low Temperature Science, Hokkaido University*

[4] *National Research Institute for Earth Science and Disaster Resilience*

[5] *Avangnaq Arctic Project*

An Automatic Weather Station (AWS) was installed at an elevation of 944 m above sea level (SIGMA-B site) on the Qaanaaq ice cap in northwestern Greenland, where continuous weather observations have been conducted since July 2012 (Aoki et al. 2014). The AWS site was estimated to have been near the equilibrium line from 2012 to 2016 based on the results of fixed-point stake observations at different elevations at the Qaanaaq ice cap (Tsutaki et al., 2017). However, amounts of accumulation and ablation at this site and their temporal variation have not been quantified. The mass loss in the low-elevation coastal ice cap is significantly higher than that in the inland ice cap due to the recent temperature rising (Noël et al., 2017), and it is therefore important to quantitatively verify a temporal variation of the surface mass balance at this site.

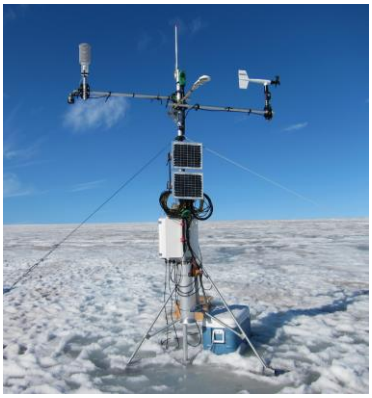

Figure 1. Overview of the AWS system and the ambient environment at SIGMA-B site.

In this study, we investigated the interannual variation of surface energy balance and surface melting rate at the SIGMA-B site to understand the present condition of the snow/ice surface and its accumulation/ablation process based on the ground meteorological observation data obtained over several years at the site.

We used hourly observation data of air temperature, relative humidity, wind direction, wind speed, atmospheric pressure, upward/downward shortwave, and longwave radiations, and snow depth observed by AWS at the SIGMA-B site (77.518° N, 69.062° W) on the Qaanaaq ice cap located in northwest Greenland (Fig. 1). Data from July 2012 to August 2020 were used for the analysis in this study.

The surface energy balance was calculated to estimate surface melt rate using Eqs. (1)–(4). This energy balance analysis included five energy components: net (downward−upward) shortwave radiation (SW_{net}), net longwave radiation (LW_{net}), sensible heat flux (H), latent heat flux (ιE), and sensible heat flux by rainfall (Q_{R}) (Eq. (1); Nishimura et al., 2021). The surface energy balance (SEB) is a variable corresponding to the residual of each energy quantity and is equal to the melt energy when the snow surface temperature is 0 °C and SEB > 0. H and ιE were calculated using the bulk aerodynamic method (Eqs. (2) and (3)). Q_{R} is calculated by Eq. (4). The precipitation data were obtained from the ECMWF ERA-5 data with every 0.25° spatial resolution (Hersbach, 2018). This study used an index of cloudiness (N_ε) (Eq. (5)) calculated using surface air temperature, relative humidity, and downward longwave radiation (Konzelmann et al., 1994; van den Broeke et al., 2004; Conway et al., 2015). The index was defined between 0 (clear-sky condition) and 1 (overcast condition). This study defined the direction of energy transport to the snow/ice surface as positive.

$$SEB = SW_{\mathrm{net}} + LW_{\mathrm{net}} + H + \iota E + Q_{\mathrm{R}}, \quad (1)$$

$$H = \rho\, C_{\mathrm{p}}\, C_{\mathrm{H}}\, U\, (T_{\mathrm{a}} - T_{\mathrm{s}}), \quad (2)$$

$$\iota E = \rho\, \iota\, C_{\mathrm{E}}\, U\, (q_{\mathrm{a}} - q_{\mathrm{s}}), \quad (3)$$

$$Q_{\mathrm{R}} = P_{\mathrm{r}}\, \rho_{\mathrm{w}}\, l_{\mathrm{w}}\, (T_{\mathrm{w}} - T_{\mathrm{s}}), \quad (4)$$

$$N_\varepsilon = (\varepsilon_{eff} - \varepsilon_{cs})/(\varepsilon_{ov} - \varepsilon_{cs}). \quad (5)$$

Radiant flux absorbed by the snow surface (R) is also defined as a total of SW_{net} and downward longwave radiation absorbed by snow ($\varepsilon LW_{\mathrm{d}}$), where ε (= 0.98; Armstrong and Brun, 2008) is the snow/ice surface emissivity. Since R is a major source of energy input, the temporal variation of it is a vital component to consider the surface energy balance.

In 2014/15, 2018/19, and 2019/20, the amount of surface melting was large (2014/15: 923, 2018/19: 976, 2019/20; 888 [mm w.e.]); the amount of melting was more than 1.4 times higher than the observation period average. In these years, higher

temperatures and lower albedo were observed. Those years were the three largest SW_{net} years during the observation period. This result suggests that the albedo feedback may have increased SW_{net} and triggered the surface melting.

The mean SW_{net}, εLW_d, and R in every year's summer and those variations are shown in Table 1 and Fig. 2. The year with the largest summer mean SW_{net} was 2019/20 (85.4 W m^{-2}), followed by 2014/15 (84.3 W m^{-2}). On the other hand, the year with the largest summer means εLW_d and R were 2018/19 (εLW_d: 271.4, R: 347.1 W m^{-2}). N_ε in the 2014/15 and 2019/20 summers were low, implying clear skies condition was dominant and N_ε in the 2018/19 summer was not low (Fig. 2b). Because downward longwave radiation increases under overcast conditions due to the additional black body radiation from cloud-cover, the snow surface was also possibly heated by a large amount of R with relatively more cloudy condition continued in the 2018/19 summer than in other two summers. Considering the largest surface melting occurred in the 2018/19 summer, not only the contribution of shortwave radiation from clear skies but also that of longwave radiation is important for the surface melting

Table 1. Mean summer (June, July, and August) radiant fluxes (SW_{net}, εLW_d, and R) in each year. Those ensemble averages and standard deviations are also listed in the bottom.

Year (JJA)	SW_{net} W m^{-2}	εLW_d W m^{-2}	R W m^{-2}
2011/12	64.7	267.5	349.0
2012/13	52.9	265.4	317.1
2013/14	56.8	273.4	330.0
2014/15	**84.3**	**252.8**	**336.0**
2015/16	66.3	268.2	335.0
2016/17	59.8	262.9	323.6
2017/18	53.4	265.9	319.6
2018/19	**74.4**	**271.4**	**347.1**
2019/20	**85.4**	**255.1**	**339.3**
average	66.4	264.7	333.0
SD	11.7	6.5	10.7

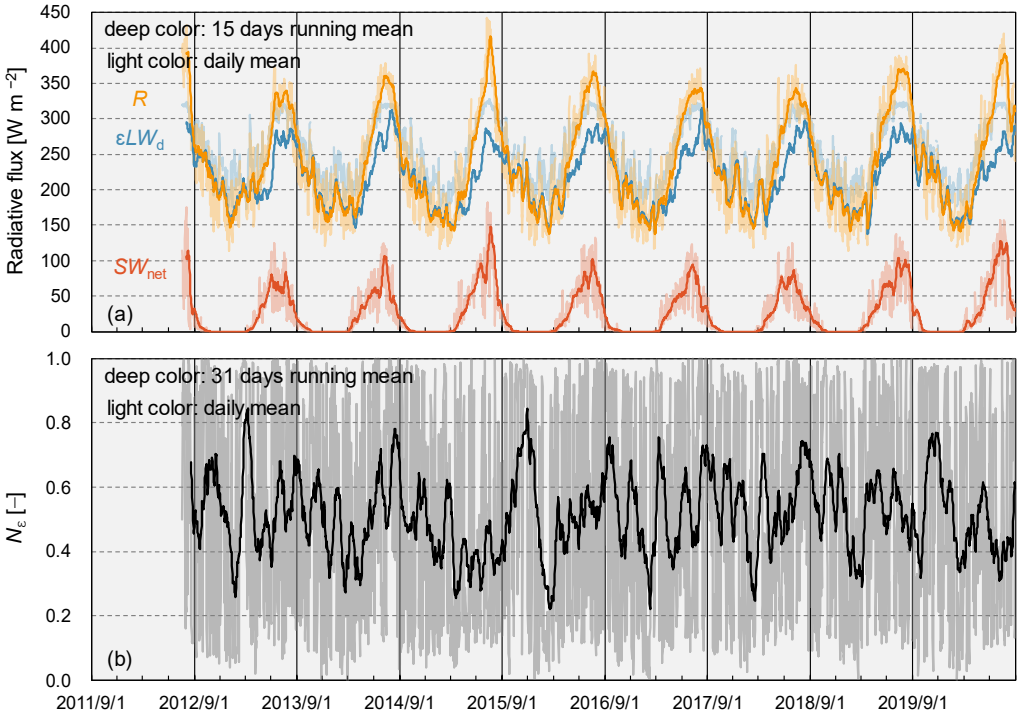

Figure 2. (a) Variation of daily mean net shortwave radiation (SW_{net}), downward longwave radiation (LW_d), and their combined input total radiation ($R^{\downarrow}$). (b) Variation of daily mean cloud cover index.

References

Aoki, T. et al., Bull. Glaciol. Res., 32, 3–20. https://doi.org/10.5331/bgr.32.3, 2014.

Armstrong, R. L. and Brun, E. (Eds.).: Physical processes within the snow cover and their parameterization, Snow and Climate: Physical Processes, Surface Energy Exchange and Modeling, Cambridge University Press, Cambridge N.Y., p. 58, 2008.

Conway, J. P. and Cullen, N. J., Int. J. Climatol., 35, 699–713. https://doi.org/10.1002/joc.4014, 2015.

Hersbach, H. et al., ERA5 hourly data on single levels from 1959 to present. Copernicus Climate Change Service (C3S) Climate Data Store (CDS). (Accessed on September 12, 2022), 10.24381/cds.adbb2d47, 2018.

Konzelmann, T. et al., Global Planet. Change, 9, 143–164. https://doi.org/10.1016/0921-8181(94)90013-2, 1994.

Nishimura, M. et al., Environ. Res. Comm., 3(051003), 1–16. https://doi.org/10.1088/2515-7620/abfcae, 2021.

Noël, B. et al., Nat. Comm., 8(14730). https://doi.org/10.1038/ncomms14730, 2017.

Tsutaki, S. et al., Ann. Glaciol., 58, 181–192. https://doi.org/10.1017/aog.2017.7, 2017.

van den Broeke M. R. et al., Journal of. Atmospheric. Oceanic Technology. 21: 1417–1431, https://doi.org/10.1175/1520-0426(2004)021<1417:AAITQO>2.0.CO;2., 2004.